Stream-discharge surges generated by groundwater flow

Supporting information

Adrien Guérin[1], Olivier Devauchelle[1], Vincent Robert[1], Thierry Kitou[1],

Céline Dessert[1], Amélie Quiquerez[2], Pascal Allemand[3], and Eric Lajeunesse[1]

[1]Institut de Physique du Globe de Paris, Sorbonne Paris Cité, Université Paris Diderot, UMR 7154 CNRS, 1 rue Jussieu, 75238 Paris, Cedex 05, France

[2]Université de Bourgogne, UMR CNRS 6298, ARTeHIS, 6 Boulevard Gabriel, 21000 Dijon, France

[3]Université Claude Bernard Lyon 1, Ens de Lyon, CNRS, UMR 5276 LGL-TPE, F-69622, Villeurbanne, France

Contents of this file

Text S1. Field Site

The Quiock creek is a small tributary of the Bras-David river, draining a catchment of about 7.9 hectares on the volcanic island of Basse-Terre in the Guadeloupe Archipelago, Lesser Antilles. Using a 5×5 m digitised elevation model (Litto3D®), and the Whitebox

Corresponding author: Olivier Devauchelle, devauchelle@ipgp.fr

Geospatial Analysis Tool (Lindsay, 2016), we find that about $L_r = 0.98\,\mathrm{km}$ of channels drain the Quiock catchment upstream of our discharge gauge, located at 16° 10′ 36″ N, 61° 41′ 44″ W.

Between January 2015 and October 2017, we recorded an average annual rainfall rate of about $2490\,\mathrm{mm\,yr^{-1}}$ under the vegetation cover (Text S2). Another gauge, located in a clearing about half a kilometer away from the catchment, recorded an average rainfall rate of about $3140\,\mathrm{mm\,yr^{-1}}$, indicating a throughfall of almost 80 %. Over the same period, the average discharge of the Quiock creek was $11.2\,\mathrm{m^3\,h^{-1}}$. Apportioned to the catchment area, this corresponds to a specific discharge of $1250\,\mathrm{mm\,yr^{-1}}$. We thus estimate that the sum of evapotranspiration and deep groundwater recharge represents about 60 % of the rainfall rate (Clergue et al., 2015).

The Quiock creek drains a thoroughly weathered aquifer (Guérin, 2015). A 12.5-m deep borehole revealed a homogeneous ferralitic soil, composed mostly of clay (about 70 %, mainly halloysite and kaolinite) and iron hydroxide (about 19 % of Fe(III)-hydroxides) (Buss et al., 2010). Primary minerals (quartz, feldspar and cristobalite) make up the rest of the aquifer, mostly in the first 30 cm beneath the surface (Clergue et al., 2015). This ferralitic regolith, which develops on Pleistocene andesitic pyroclastic deposits, is often more than 15-m thick on Basse-Terre. It is typically moderately permeable (hydraulic conductivity of about $10^{-6}-10^{-5}\,\mathrm{m\,s^{-1}}$) and porous (total porosity of about 50 %) (Colmet-Daage & Lagache, 1965; Dorel, Roger-Estrade, Manichon, & Delvaux, 2000). We expect that both the drainable porosity and the fillable porosity of the aquifer will be much lower than the total porosity.

We performed an electric resistivity tomography (Samouëlian, Cousin, Tabbagh, Bruand, & Richard, 2005) (ERT) of a transect perpendicular to the Quiock creek, about 50 m downstream of the piezometric boreholes (Guérin, 2015). To do so, we arranged 48 electrodes along the transect, 1-m apart from each other (Wenner-Schlumberger configuration). This setup allowed us to invert for the electric resistivity field down to 6 m below the surface (Figure S1). This profile reveals a surface layer, less than 1 m-thick, with higher resistivity (400 to 900 Ω m), which corresponds to the soil horizon. Below the surface layer, the resistivity fluctuates around 200 Ω m, a value compatible with clay (Buss et al., 2010).

We have drilled six boreholes along our ERT transect, down to 6 m below the surface. The extracted material is homogeneous, with a clayey texture speckled with grains of quartz, feldspar and iron oxide. Both the resistivity transect and the borehole samples suggest that the material that makes up the Quiock creek aquifer is fairly uniform. This, however, does not ensure that its hydraulic conductivity and porosity are homogeneous as well. For instance, we expect unconsolidated clay to become less permeable and less porous with depth, due to compaction under its own weight (Ellis & Atherton, 2003; Johnson, 1967). Local measurements of these properties are notoriously challenging, since drilling alters the mechanical properties of samples, and hydraulic conductivity depends on the scale it is measured at (Keller, Van Der Kamp, & Cherry, 1989).

Text S2. Field Measurements

Water Table

We drilled seven piezometric wells with an auger, and inserted a PVC pipe (8 cm in diameter) into each of them (Figure 1c in main document). Small holes puncture the pipe's lowermost twenty centimeters. Near the bottom of each well, we placed a pressure transducer (CS451, Campbell Scientific, precision 5 mm) connected to a data logger (CR800, Campbell Scientific, resolution 1 mm). Each sensor is approximately 15 cm above the bottom of its borehole. We then measured the ground elevation along the boreholes array with a laser range finder, and calculated the elevation of the sensors relative to that of the river.

Stream Discharge

We placed the eighth pressure transducer in a Venturi flume (exponential cross section, ISMA Type III). A calibrated polynomial relates the discharge to the water depth in the flume. Manufacturing induces a 3% systematic uncertainty on this calibration (manufacturer value). The flume accommodates a broad range of discharges, from $0.93\,\mathrm{m^3\,h^{-1}}$ to $93\,\mathrm{m^3\,h^{-1}}$. We focus the stream into the canal with a concrete dam. A discharge stronger than $76\,\mathrm{m^3\,h^{-1}}$ causes overflow.

Rainfall

A tipping-bucket rain gauge (ARG100, Campbell Scientific), placed less than ten metres downstream of the boreholes, measures the rainfall rate below the vegetation cover. Rainfall fills a bucket which tips over after the total rainfall reaches 0.2 mm. Every two minutes, we record how many times the bucket has tipped over. We then divide the accumulated volume by the sampling-time interval to get the rainfall rate.

Text S3. Selection of rainfall events

The storm flow regime, of which equation (5) in the main document is the mathematical expression, holds only for an isolated rainfall event. To identify a collection of such events in our data set, we first consider the rainfall signal, and treat as an individual event any period of rainfall bracketed by dry periods. Among these, we pick the isolated events by requiring that the amount of rain fallen up to two hours before, and after, the event be less than one fifth of the amount fallen during the event proper. This procedure selects 492 isolated rainfall events in our entire data set.

Next, we characterize each event with its intensity, R_s, and the total height of rainwater fallen during the event, H_s (Figure 3a, main document). The latter is simply the integral of the rainfall rate over the event's duration. To compute R_s, we first calculate the square root of the second-order moment of the rainfall signal. By multiplying this duration by $2\sqrt{3}$, we find the duration T_s of the rectangle signal that shares the same second-order moment. Dividing H_s by this duration yields R_s.

To each isolated rainfall event should correspond a surge in the stream discharge, and therefore a peak in the time derivative of the discharge (Figure 3b, main document). To identify these peaks, we search the time series using wavelet transform-based pattern matching (Du, Kibbe, & Lin, 2006, `find_peaks_cwt` from the `scipy.signal` Python library). We then discard any event for which, during the T_s-long rain period, we find more than one peak, or no peak at all. For the 168 remaining events, we define the amplitude of the discharge surge ΔQ_s as the difference between the highest and lowest values of the discharge during the T_s-long period centered around the peak.

The main uncertainty about the discharge surge ΔQ_s are fluctuations of the water elevation measurements in the flume, which amplitude is about the measurement resolution. Multiplying this value with the derivative of the calibrated polynomial yields an estimate of the uncertainty. We filter out of our data set any event which discharge surge is lower than this uncertainty, or which total height of rainwater is lower than the resolution of the rain gauge. After this procedure, we are left with the 137 events displayed in Figure 3c (main document).

Text S4. Propagation of the Rainfall Signal Through the Vadose Zone

Before the water table can react to a rainfall event, the information that fresh rainwater recharges the aquifer needs to travel through the vadose zone, either in the form of rainwater itself percolating down to the water table, or of a wetting front traveling towards it. Only when this signal has reached the water table can the pressure induced by rainfall push more groundwater into the stream. In principle, the rainfall, groundwater-level and stream-discharge time series should allow us to monitor these steps.

To do so, we turn again to the 137 isolated rainfall events of the main document (Figure 3, Sec. 3). To each event, we now associate three times: t_R for the rainfall event itself, t_{WT} for the water table reaction to the event, and t_Q for the associated surge in stream discharge. We expect the time lag between the rainfall and the water-table rise, $t_{WT} - t_R$, to inform us about the travel of the rain signal through the vadose zone. Conversely, we expect virtually no delay between t_Q and t_{WT}, as pressure propagates at the speed of sound through the saturated zone.

In accordance with our simplified representation of a rainfall event (Figure 3a in main document), we define the time of the event as the normalized first moment of the rainfall time series:

$$t_R = \frac{\int R(t)\, t\, \mathrm{d}t}{\int R(t)\, \mathrm{d}t}\,. \tag{1}$$

By definition, t_R is the midtime of the rain event.

We identify the time of the discharge surge, t_Q, to the corresponding peak of the time derivative of the discharge (Text S3). Likewise, we define t_{WT} as the time of fastest water-table rise. To find it, we simply apply to the time series of the borehole level the procedure designed for the discharge surge (Sec. 3).

The stream discharge is a sharper signal than the water-table level, which variations appear to be smoothed out by either the groundwater flow or our measurement device. In combination with the limited resolution of the pressure gauge, this causes our peak-detection procedure to miss many small events in the water-table signal. Among all the rainfall events of Figure 3 (main document), only 54 induce a perceptible water-table rise. Figure S2a shows these events in the time-lag space, the coordinates of which are the reaction times of the water table and of the stream discharge. The data points are broadly distributed around the origin, with a comparable dispersion along both coordinates (Figure S2b,c).

On average, we find that the water table raises a few minutes after the rain event ($\langle t_{WT} - t_R \rangle = 4.0 \pm 1.6$ minutes, where $\pm$ indicates error on the mean). As for the stream discharge, it appears to raise the fastest a few seconds before the midtime of the rain event ($\langle t_Q - t_R \rangle = -0.79 \pm 1.4$ minutes). Both values are smaller than the standard deviation

(about 10 minutes), and the best we can say is that both the water table and the stream discharge react within minutes of a rain event. Typically, just before a rain event, the water table lies a few meters below the ground surface, suggesting the rain signal travels at a few millimeters per second through the vadose zone. This velocity compares with K/ϕ_f, an estimate of the expected infiltration rate in the Quiock aquifer.

Text S5. Boussinesq Approximation

The Boussinesq approximation combines Darcy's law with the shallow-water approximation to state that the horizontal groundwater velocity, v_g, is proportional to the gradient of the water-table elevation (Bear, 2013; Boussinesq, 1904; Dupuit, 1848):

$$v_g = -K\frac{\partial h}{\partial x} \tag{2}$$

where K is the (vertically-averaged) hydraulic conductivity. The groundwater flux associated to this flow is hv_g. When the aquifer is being recharged at rate R (which may well vanish), the groundwater balance reads

$$\phi\frac{\partial h}{\partial t} = \frac{K}{2}\frac{\partial^2 h^2}{\partial x^2} + R\,, \tag{3}$$

where t is time, and ϕ is the porosity (other notations are those of the main paper). When the water table rises ($\partial h/\partial t > 0$), the porosity is the fillable porosity ϕ_f. Conversely, when the water table receeds, it is the drainable porosity ϕ_d. Assuming that most of the groundwater flow occurs above the stream level means, mathematically, that h vanishes along the drainage network, that is, at $x = 0$. Finally, by definition, the groundwater flux vanishes across a divide, that is, $\partial h/\partial x = 0$ at $x = L_a$.

Averaging the above equation over a sufficiently long period yields

$$\frac{K}{2}\,\frac{\partial^2}{\partial x^2}\,h_{\mathrm{RMS}}^2 + \langle R\rangle \approx 0\,, \tag{4}$$

of which equation (1) in the main document is a solution.

To compare our piezometric observations with equation (1) of the main document, we first average the square elevation of the water table over our entire data set (from January 14, 2015 to October 19, 2017). Taking the square root of the result yields the root mean square elevation of the water table in each borehole, h_{RMS}. Evaluating L_a based on the digital elevation model of the Quiock catchment (Figure 1a, main document), we then fit the coefficient $\langle R\rangle/K$ to our data (Figure 1c, main document). Repeating this procedure for the three years of our data set independently, we get three evaluations of the hydraulic conductivity K, namely 4.6×10^{-6}, 6.3×10^{-6} and $7.2\times10^{-6}\,\mathrm{m\ s^{-1}}$, respectively. We thus estimate our uncertainty about the hydraulic conductivity to be of the order of 30 %.

Text S6. Recession Flow

Among the classical predictions of the Boussinesq approximation is the recession of the aquifer's discharge during a prolonged drought (Brutsaert & Nieber, 1977). This regime is commonly used to estimate the representative hydraulic conductivity and drainable porosity of an aquifer at the catchment's scale (Rupp, Schmidt, Woods, & Bidwell, 2009). At the end of a drought flow, the water table approaches a classical self-similar solution of equation (3):

$$h(x,t) = \frac{L_a^2\,\phi_d}{K\,(t-t_0)}\,\mathcal{H}_d\left(\frac{x}{L_a}\right)\,, \tag{5}$$

where $\mathcal{H}_d$ is the dimensionless profile of the water-table elevation; it satisfies an ordinary differential equation without any parameter (Polubarinova-Kochina, 1962):

$$\mathcal{H}_d \, \mathcal{H}_d'' + \mathcal{H}_d'^2 + \mathcal{H}_d = 0 \, . \tag{6}$$

In most cases, one does not need to solve the above equation; that it has a solution such that $\mathcal{H}_d = 0$ at the stream ($x/L_a = 0$) and $\mathcal{H}_d' = 0$ at the divide ($x/L_a = 1$) suffices. The actual expression of a self-similar solution (here, Eq. (5)) is often the most useful element of an asymptotic regime (Barenblatt, 1996). Here, we will nonetheless use the value of $\mathcal{H}_d$ at the specific position x of piezometer G. In Eq. (5), t_0 is the integration constant that defines the critical time at which the asymptotic regime diverges. In practice, however, t_0 is just a fit parameter, and the asymptotic regime holds only long after the mathematical singularity.

Injecting this self-similar solution into the expression of the groundwater flux, Eq. 2, and multiplying the result by the total stream length in the catchment, L_r, we find that the groundwater discharge during the recession flow reads

$$Q = C_d \, \frac{\phi_d^2 \, L_r \, L_a^3}{K \, (t - t_0)^2} \tag{7}$$

where $C_d \approx 1.39$ is a mathematical constant, whose value is defined by the solution to Eq. (6) (Brutsaert, 2005):

$$C_d = 2 \mathcal{H}_d' \, \mathcal{H}_d \quad \text{at} \quad \frac{x}{L_a} = 0 \, . \tag{8}$$

During a drought, the recession of the discharge follows that of the water table. Accordingly, equations (5) and (7) share the same critical time, t_0.

To identify the drought flow regime in the Quiock catchment, we first select the longest drought period in our time series, which took place between January and March 2015 (Figure S3). We now need to simultaneously fit equations (5) and (7) to our observations. This fit involves three parameters in total: the critical time t_0, which is common to the two equations, and two amplitudes, A_h and A_Q, which characterize the decline of the water table (Eq. (5)) and of the groundwater discharge (Eq. (7)), respectively.

Let us consider first the recession of the water table (Figure S3a). To keep the procedure simple, we only use the furthest piezometer from the stream, where we expect the strongest signal (borehole G). The fit of equation (5) to this time series is non-linear, and therefore can lead to multiple optima. To rule out this possibility, we first choose a critical time t_0, and use the method of least squares to adjust the amplitude A_h, such that

$$h = \frac{A_h}{t - t_0} \tag{9}$$

is a proper fit of the data. We then calculate the associated error and repeat this procedure for a series of critical times. The errors then show a single, unambiguous minimum around $t_0 = 46$ days before the beginning of the time series. The associated amplitude of the asymptotic regime is $A_h = 175\,\mathrm{m\,day}$. The theoretical recession then accords with our observations (Figure S3a).

Fitting the amplitude of equation (7) on the hydrograph of the Quiock creek is now straightforward (Figure S3b). Using the critical time t_0 of the water-table recession, we use the method of least squares to adjust the amplitude A_Q such that

$$Q = \frac{A_Q}{(t - t_0)^2} \tag{10}$$

is close to the discharge time series. We find that an amplitude of $A_Q = 2.8 \times 10^4\,\mathrm{m^3\,h^{-1}\,day^2}$ best fits our data. The combination of daily oscillations and minute rain events makes the hydrograph recession noisier than that of the water table. The theory, nonetheless, closely follows the trend of the stream discharge.

The advantage of measuring simultaneously the recession of both the water table and the stream discharge becomes apparent when combining equations (5) and (7), which yields an estimate of the characteristic drainable porosity of the aquifer:

$$\phi_d = \frac{A_Q}{A_h} \frac{\mathcal{H}_d(x/L_a)}{C_d\, L_r\, L_a}\,, \tag{11}$$

where x is the distance between the stream and the borehole ($x = 29.2\,\mathrm{m}$ for borehole G). Using this formula, we find $\phi_d \approx 5.3 \cdot 10^{-2}$, about four times the value of the fillable porosity, ϕ_f, deduced from the storm flow regime (equation (5) in the main document).

The same reasoning also provides the expression of the representative hydraulic conductivity:

$$K = \frac{A_Q}{A_h^2} \frac{L_a\, \mathcal{H}_d^2(x/L_a)}{L_r\, C_d}\,, \tag{12}$$

which yields $K \approx 4.1 \cdot 10^{-6}\,\mathrm{m\,s^{-1}}$ in the Quiock catchment, a value fairly close to the one deduced from the average water-table shape (equation (1) in the main document).

Text S7. Storm Flow Regime

The storm flow regime is an asymptotic solution of the Boussinesq equation (3) under constant forcing by rainfall (Guérin, Devauchelle, & Lajeunesse, 2014). In its idealized formulation, it begins with an empty aquifer ($h = 0$ initially). At time $t = 0$, a storm occurs, and sustains a constant rainfall rate, R_s, for a period T_s. The solution to this

mathematical problem is, like the recession flow (5), a self-similar regime. Unlike the recession flow, however, it is valid only just after the storm has begun. Its analytical expression reads

$$h_s = \frac{R_s\, t}{\phi_f}\, \mathcal{H}_s \left(\frac{\phi_f\, x}{t} \sqrt{\frac{2}{K R_s}} \right) \tag{13}$$

where $\mathcal{H}_s$ is, like $\mathcal{H}_d$, the solution of an ordinary differential equation without any parameter (Guérin et al., 2014):

$$\mathcal{H}_s\, \mathcal{H}_s'' + \mathcal{H}_s'^2 + \frac{1}{2} \left(\mathcal{X}\, \mathcal{H}_s' - \mathcal{H}_s + 1 \right) = 0\,, \tag{14}$$

where $\mathcal{X}$ is the self-similar variable of $\mathcal{H}_d$, which combines time and space into a single expression:

$$\mathcal{X} = \frac{\phi_f\, x}{t} \sqrt{\frac{2}{K R_s}}\,. \tag{15}$$

That the self-similar variable is proportional to the ratio x/t, by itself, indicates that the corresponding profile of the water table will feature a front growing away from the stream. Like for the classical recession flow (Sec. S6), the scalings involved in Eq. (13) matter more, in practice, than the full solution to Eq. (14). Nonetheless, Fig. 2 (main document) shows a numerical approximation of the latter. The same solution is represented at successive times, to illustrate the evolution of the water table in the storm-flow regime, with parameters values that are typical for the Quiock aquifer. Far from the outlet, the water table rises like $R_s\, t/\phi_f$, unaffected by the stream's presence. It remains flat, and the aquifer accommodates the flux of rainwater uniformly.

Near the outlet, however, the water table needs to remain at the stream's level—or, equivalently, to remain at atmospheric pressure. In the framework of the Boussinesq

approximation, this translates into $h_s = 0$ at the aquifer's outlet. The water table satisfies this boundary condition by maintaining a curved front near the stream. Being self similar, Eq. (13) ensures that this front preserves its shape as the water table rises.

Using equation (13), we now calculate the discharge delivered to the stream during the storm flow regime, Q_s. To do so, we derive h_s^2 with respect to x near the stream, and multiply the resulting flux by the hydraulic conductivity K, and by the length of the aquifer's boundary—roughly twice that of the drainage network, L_r:

$$Q_s = \frac{a^2 L_r}{\phi_f} \sqrt{2K}\, R_s^{3/2}\, t\,, \tag{16}$$

where a is a mathematical constant, derived from a numerical solution of Eq. (14):

$$a = \sqrt{2\mathcal{H}_s' \mathcal{H}_s} \quad \text{at} \quad \frac{x}{L_a} = 0\,. \tag{17}$$

We are not aware of any analytical expression for this constant, but approaching it numerically is straightforward; one then finds $a \approx 1.016$ (Guérin et al., 2014).

Finally, we equate the discharge surge, ΔQ_s, with the discharge at the end of the storm regime, at $t = T_s$. It is then a matter of algebraic manipulation to derive equation (5) (main document), where the numerical prefactor is defined as

$$C = \frac{\pi a^2}{4\sqrt{2}} \approx 0.57\,. \tag{18}$$

Text S8. Initial groundwater state

None of the rainfall events in our data set begins after a drought long enough to empty the aquifer entirely—the Quiock stream seldom dries out. In that sense, none of these events are truly isolated from the previous ones, and the initial state of the groundwater flow could affect the stream's response to rainfall (Biswal & Nagesh Kumar, 2014; Botter,

Porporato, Rodriguez-Iturbe, & Rinaldo, 2009; Kirchner, 2009). Here, we evaluate this influence by considering the correlation between the observed prefactor of equation (5) (main document), and the stream's discharge before an event, Q_i, or the elevation of the water table at the same time, h_i. Like in sections S4 and S6, we consider the elevation of the watertable in borehole G (figure 1, main document).

We first detrend the data of figure 3 (main document) by dividing the normalized discharge surge, $\Delta Q_s/\langle Q\rangle$, by the intensity of the recharge, $(R_s/\langle R\rangle)^{3/2}T_s$. We then plot the resulting quantity, which should be C/T_c after equation (5) (main document), as a function of the initial state of the aquifer (figure S4). We expect that, when the groundwater is in the storm-flow regime, the two quantities will show no correlation.

Strictly speaking, the storm-flow regime applies when the aquifer is virtually empty before the rain starts. Mathematically, this requires that the discharge before the event be negligible with respect to the discharge surge, that is, that $Q_i/\Delta Q$ be small. We find virtually no correlation between this ratio and the stream's response, even when the former is larger than one (Pearson correlation coefficient of -0.026, figure S4**a**). However, a stronger mathematical condition for the applicability of the storm-flow regime is that the rainfall event occurs during a drought, that is, when $Q_i/\langle Q\rangle$ is small. Figure S4**b** shows a stronger correlation between the stream's response and this ratio (Pearson correlation coefficient of 0.58), indicating that the initial state of the aquifer changes the latter's response to the rainfall signal.

We define the most isolated events as those for which $Q_i/\langle Q\rangle$ is less than 0.1 (empty markers in figure S4). This restrictive definition reduces our data set to 10 events, for

which the storm-flow regime is most likely to apply. For this smaller data set, we find an average characteristic time of $T_c = 49\,\text{days}$—perhaps a better estimate of the actual value, although less reliable statistically (dashed red line in figure S4).

Finally, we represent the initial state of the aquifer with the elevation of the water table before the rainfall event, h_i, and repeat the above analysis. As explained in section 4, this reduces our data set to the 54 events (3 very isolated events) shown on figures S4**c** and S4**d**. Again, the correlation is probably insignificant when h_i is normalized with the amplitude Δh (correlation coefficient of -0.30), and appears somewhat stronger when h_i is normalized with its root mean square value, h_{RMS} (correlation coefficient of 0.49).

In conclusion, we find that, in general, the initial state of the aquifer changes its response to a rainfall event, in accordance with both previous observations and the Boussinesq approximation (Biswal & Nagesh Kumar, 2014; Botter et al., 2009; Kirchner, 2009). As expected, however, when the storm-flow regime is most likely to hold—that is, after a prolonged drought—we do not see any correlation with the initial state of the aquifer (empty markers in figures S4**b** and S4**d**), although our data set for such isolated events is too thin for a definitive conclusion.

References

Barenblatt, G. I. (1996). *Scaling, self-similarity, and intermediate asymptotics: dimensional analysis and intermediate asymptotics* (Vol. 14). Cambridge University Press.

Bear, J. (2013). *Dynamics of fluids in porous media*. Courier Corporation.

Biswal, B., & Nagesh Kumar, D. (2014). Study of dynamic behaviour of recession curves. *Hydrological Processes*, *28*(3), 784–792.

Botter, G., Porporato, A., Rodriguez-Iturbe, I., & Rinaldo, A. (2009). Nonlinear storage-discharge relations and catchment streamflow regimes. *Water resources research*, *45*(10).

Boussinesq, J. (1904). Recherches théoriques sur l'écoulement des nappes d'eau infiltrées dans le sol et sur le débit des sources. *Journal de mathématiques pures et appliquées*, 5-78.

Brutsaert, W. (2005). *Hydrology: an introduction*. Cambridge Univ Pr.

Brutsaert, W., & Nieber, J. L. (1977). Regionalized drought flow hydrographs from a mature glaciated plateau. *Water Resources Research*, *13*(3), 637-643.

Buss, H. L., White, A. F., Dessert, C., Gaillardet, J., Blum, A. E., & Sak, P. B. (2010). Depth profiles in a tropical volcanic critical zone observatory: Basse-terre, guadeloupe. In *Proc. of the 13th intl. symp. on water–rock interaction.*

Clergue, C., Dellinger, M., Buss, H. L., Gaillardet, J., Benedetti, M. F., & Dessert, C. (2015). Influence of atmospheric deposits and secondary minerals on li isotopes budget in a highly weathered catchment, guadeloupe (lesser antilles). *Chemical Geology*, *414*, 28-41. doi: 016/j.chemgeo.2015.08.015

Colmet-Daage, F., & Lagache, P. (1965). Caractéristiques de quelques groupes de sols dérivés de roches volcaniques aux antilles françaises. *Cahiers de l'ORSTOM serie pédologie*, *8*, 91-121.

Dorel, M., Roger-Estrade, J., Manichon, H., & Delvaux, B. (2000). Porosity and soil water properties of caribbean volcanic ash soils. *Soil Use and Management*, *16*(2), 133–140.

Du, P., Kibbe, W. A., & Lin, S. M. (2006). Improved peak detection in mass spectrum by incorporating continuous wavelet transform-based pattern matching. *Bioinformatics*, *22*(17), 2059-2065. doi: 10.1093/bioinformatics/btl355

Dupuit, J. (1848). *Etudes theoriques et pratiques sur le mouvement des eaux courantes*. Carilian-Goeury.

Ellis, S., & Atherton, J. (2003). Properties and development of soils on reclaimed alluvial sediments of the humber estuary, eastern england. *Catena*, *52*(2), 129–147.

Guérin, A. (2015). *Dynamics of groundwater flow in an unconfined aquifer* (Doctoral dissertation, Université Paris Diderot (Paris 7), Sorbonne Paris Cité). Retrieved from `https://hal.archives-ouvertes.fr/tel-01884762/file/manuscrit.pdf`

Guérin, A., Devauchelle, O., & Lajeunesse, E. (2014, nov). Response of a laboratory aquifer to rainfall. *Journal of Fluid Mechanics*, *759*, -1. doi: 10.1017/jfm.2014.590

Johnson, A. (1967). *Specific yield: compilation of specific yields for various materials* (Geological Survey Water-Supply Paper No. 1662-D). US Government Printing Office.

Keller, C. K., Van Der Kamp, G., & Cherry, J. A. (1989). A multiscale study of the permeability of a thick clayey till. *Water Resources Research*, *25*(11), 2299–2317.

Kirchner, J. W. (2009). Catchments as simple dynamical systems: Catchment characterization, rainfall-runoff modeling, and doing hydrology backward. *Water Resources Research*, *45*(2), n/a–n/a. Retrieved from `http://dx.doi.org/10.1029/2008WR006912` (W02429) doi: 10.1029/2008WR006912

Lindsay, J. B. (2016). Whitebox gat: A case study in geomorphometric analysis. *Com-*

puters & Geosciences, *95*, 75–84. doi: 10.1016/j.cageo.2016.07.003

Polubarinova-Kochina, P. Y. (1962). Theory of ground water movement princeton university press. *Princeton, NJ*.

Rupp, D. E., Schmidt, J., Woods, R. A., & Bidwell, V. J. (2009). Analytical assessment and parameter estimation of a low-dimensional groundwater model. *Journal of hydrology*, *377*(1-2), 143–154.

Samouëlian, A., Cousin, I., Tabbagh, A., Bruand, A., & Richard, G. (2005). Electrical resistivity survey in soil science: a review. *Soil and Tillage research*, *83*(2), 173–193.

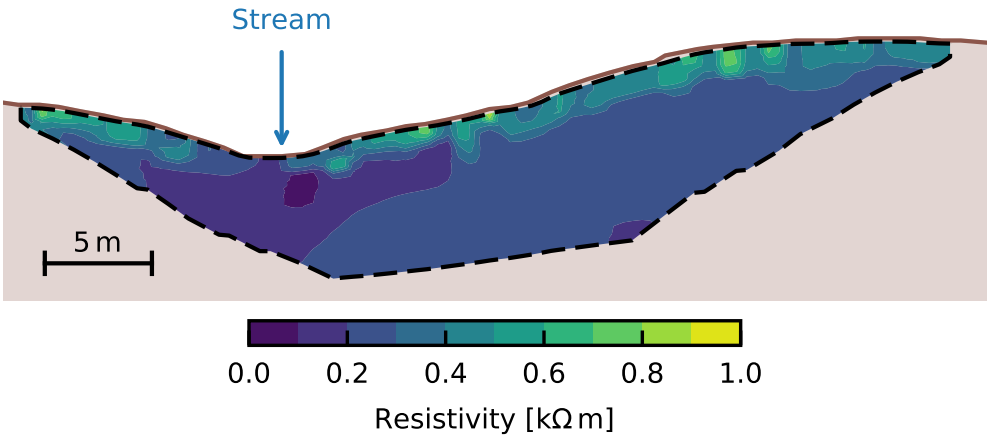

Figure S1. Electrical resistivity tomography of the Quiock aquifer. The 48 electrodes lay along a transect orthogonal to the Quiock creek, 1 m apart from each other, and 50 m downstream of the piezometer wells. Aspect ratio is preserved. Right-hand part of the transect points towards Southeast. Stream flows away from reader's eye.

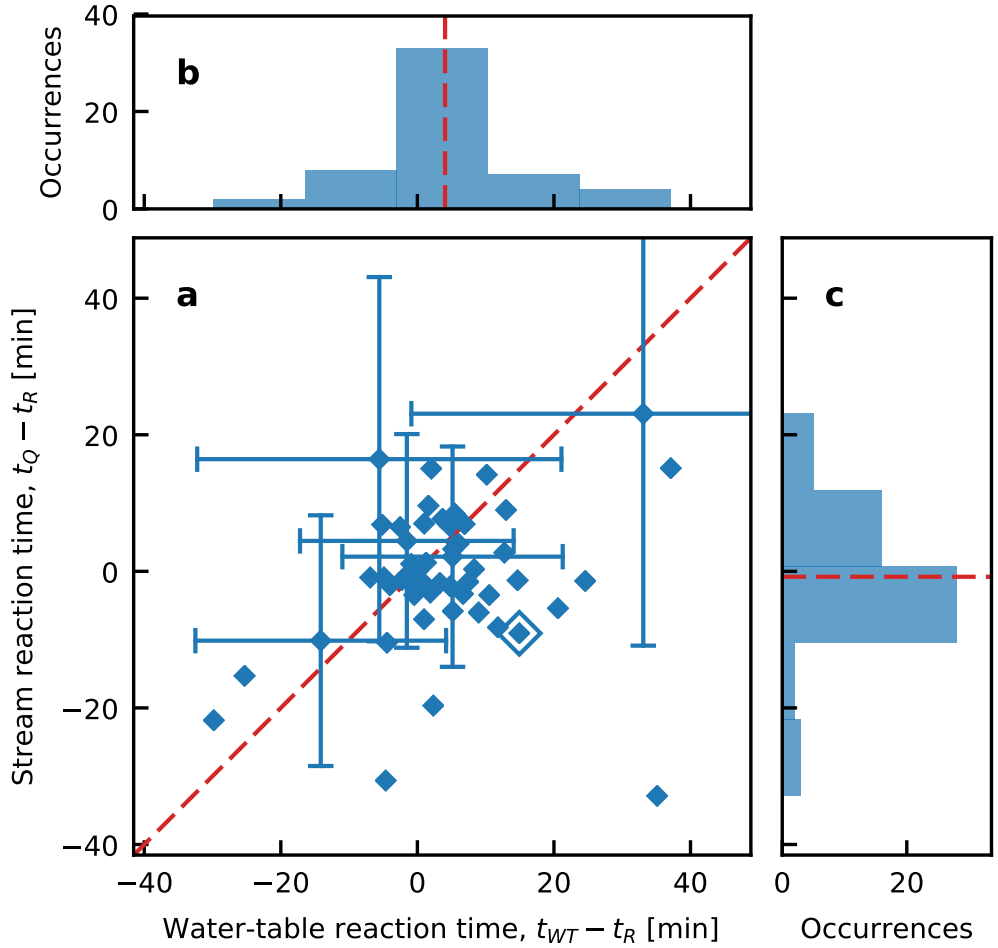

Figure S2. Reaction time of water table and stream discharge. (a) Time lag between the stream discharge and the rainfall event, $t_Q - t_R$, as a function of the water-table reaction time, $t_{WT} - t_R$, where t_R corresponds to the midtime of the rainfall event, and t_Q and t_{WT} correspond to the fastest increase of the stream discharge and water-table level, respectively. Error bars indicate the duration of the rainfall event. Rimmed marker indicates event of Figure 2a and 2b in main document. Dashed orange line: one-to-one relation. (b) Distribution of water-table reaction time. Dashed orange line: average reaction time. (c) Distribution of stream reaction time. Dashed orange line: average reaction time.

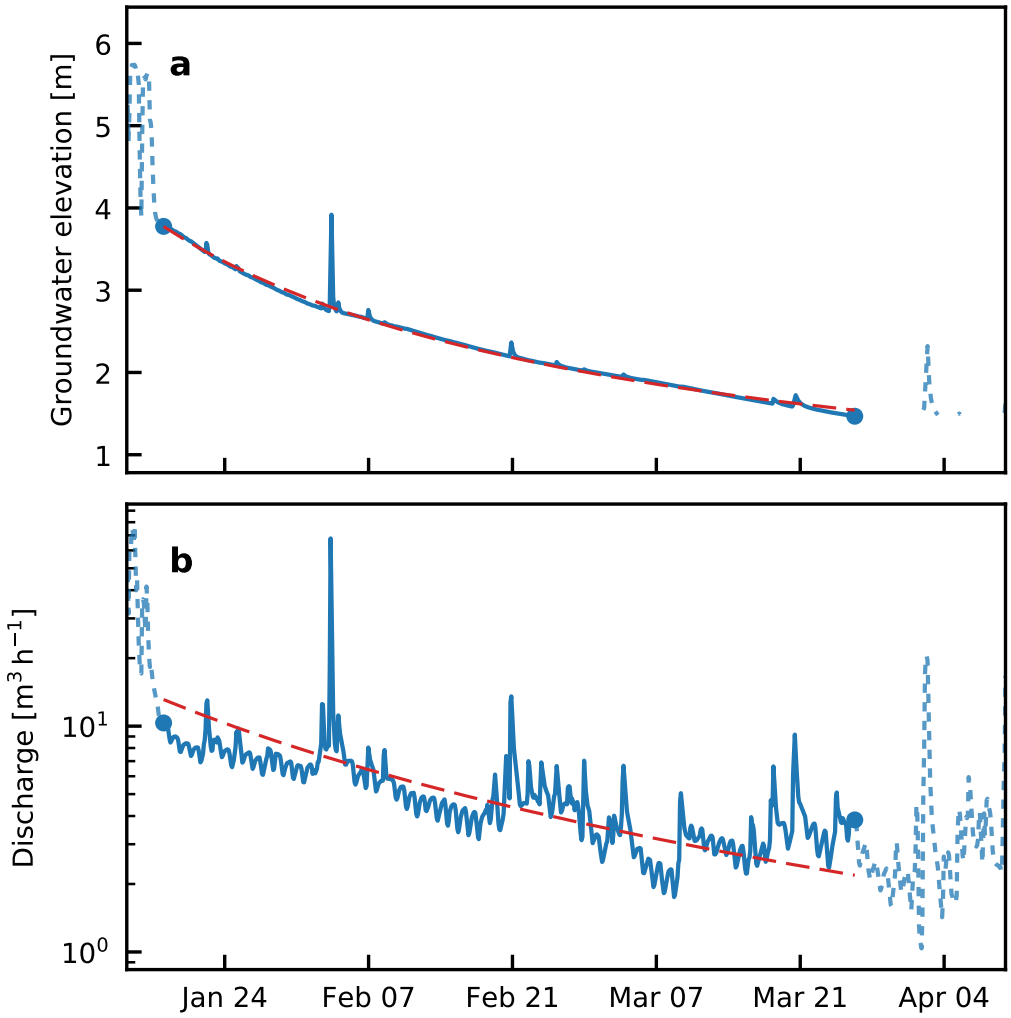

Figure S3. Recession of the Quiock aquifer during a drought. (a) Water-table level in borehole "G" (Figure 1c in main document) as the aquifer drains into the Quiock creek (blue line). Elevation is relative to stream elevation. Darker blue indicates range over which theory is fitted. Orange dashed line: equation (5) fitted to observations. No line: water table below sensor. (b) Evolution of the stream discharge (blue line). Solid line indicates range over which theory is fitted. Orange dashed line: equation (7) fitted to observations.

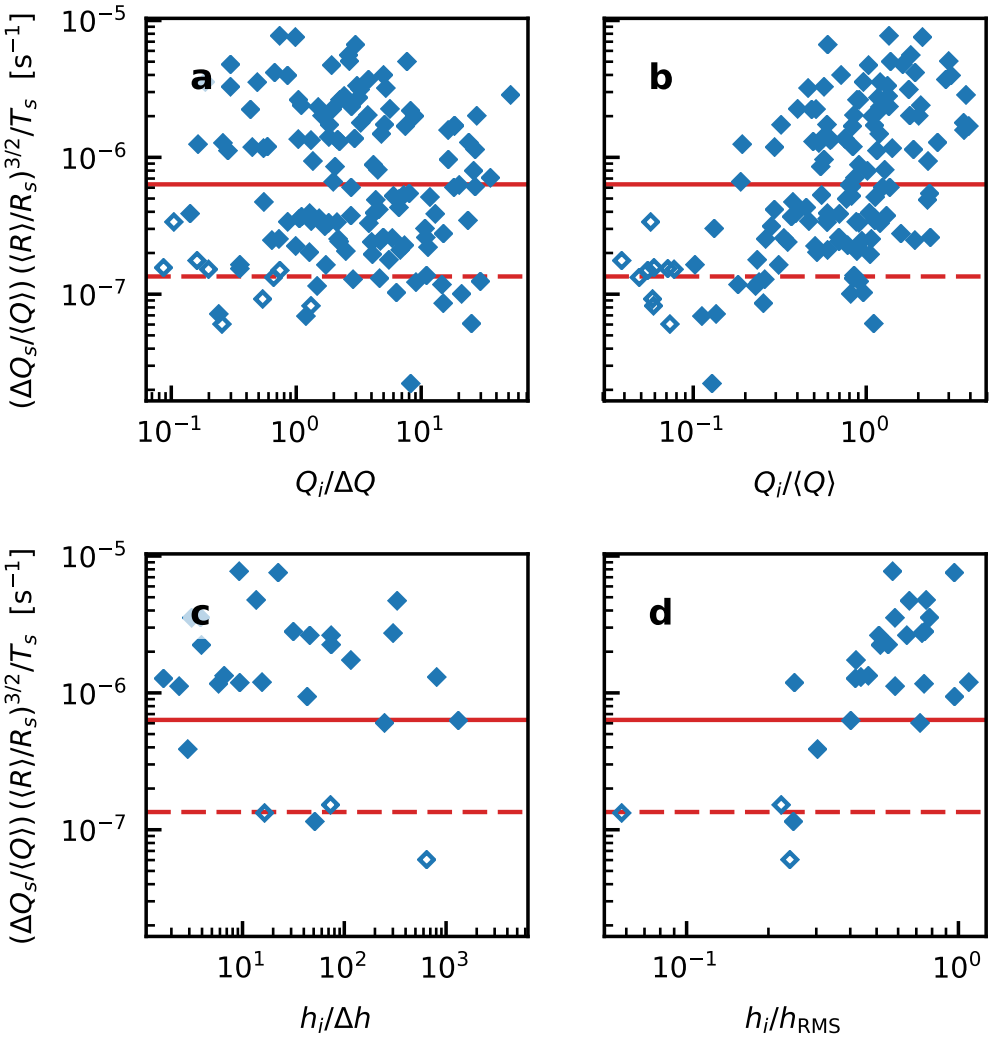

Figure S4. Influence of groundwater state before rainfall on stream's response. Blue markers correspond to the rainfall events of Figure 3 (main document) (**a** and **b**), or a subset of them (**c** and **d**). Empty markers indicate very isolated events ($Q_i/\langle Q\rangle < 0.1$). Vertical axis is C/T_s, after equation (5) (main document). Solid red line is the best fit for all events ($T_c = 10.4$ days); dashed red line is the best fit for very isolated events ($T_c = 49$ days).